

Assessment of the Homogeneous Approach to Predict Unsteady Flow Characteristics of Sheet and Cloud Cavitation

Cote P and Dumas G*

LMFN Lab, Mechanical Engineering Department, Laval University, Quebec, QC G1V 0A6, Canada

Abstract

In this work, the homogeneous approach, frequently used to simulate cavitation in hydraulic machinery, is used to compute unsteady cavitating flows for two simplified geometries. After a quick review of the literature and a rigorous presentation of the proposed methodology, the detailed computed physics of sheet and cloud cavitation are compared with experimental observations and with theory. Results suggest that the assumption of a homogeneous medium is not suitable to predict the fine physics of attached cavitation and thus to predict its precise unsteady characteristics. However, the inhomogeneous approach, in which a momentum equation is solved for both phases under a volume of fluid (VOF) approach, is shown to be more promising. Although it is numerically less stable, such an approach allows the effective body to be modified by the presence of vapor in contrast with the homogeneous approach. The resulting flow topology around the vapor cavity is found to better agree with the experimental observations, and thus the inhomogeneous approach offers the potential to better predict the unsteady characteristics of attached cavitation.

Keywords: CFD; Cavitation modelling; Homogeneous approach; Unsteady flows; Sheet cavitation; Cloud cavitation

Introduction

In an era of emergence of new renewable energy technologies, hydraulic turbines become the corner stone of a complex energy market. As a quick, reliable source of renewable energy, they are operated more frequently in transient and off-design operating conditions to secure the network. As documented in Dörfler et al. [1] and further demonstrated by the works of Yakamoto [2] and Lewys [3], in off-design operating conditions, cavitation may occur and play a leading role in the dynamics of the fluid flow inside the turbine runners.

The state of the art in the simulation of cavitation relies on the assumption of a homogeneous medium which is simply characterized by a mixture volume density. The physics of vaporization and condensation are then governed by different cavitation models. The literature is rich in studies assessing the capacity of numerous cavitation models to predict steady and unsteady characteristics of cavitation with a variable degree of success. For example, the works of Arndt and Song [4], Coutier-Delgosha [5,6], Frikha [7], Ducoin [8] and Zwart [9] and many others have all proposed promising avenues in simulating sheet and cloud cavitation with the homogeneous approach under various assumptions for phase change. However, none of those works has focused on the fine flow physics associated with the homogeneous assumption close to the vapor cavity. As recalled by Brennen [10], this homogeneous assumption is only reasonable if one considers that the dispersed phase is formed of small bubbles, well mixed with the liquid and mainly transported by its convection. However, in the case of attached cavitation where a significant vapor cavity is present along the body, it is not clear if such an assumption is well suited.

The objective of the work presented in this paper is thus to assess the capabilities of the homogeneous approach implemented in a widely used commercial solver to predict the unsteady characteristics of attached cavitation on two experimentally tested setups. The results are compared to those obtained from simulations using the inhomogeneous approach on a case of attached cavitation.

Numerical Methodology

To perform the computations, the commercial solver ANSYS CFX

14.5 [11,12] is used on 1 cell thick pseudo 2-D meshes of the flow fields. In this work, cavitation is modeled through a mass transfer ideology via the Rayleigh-Plesset model included in CFX, whereas the continuity equation states that:

$$\frac{1}{\rho} \left(\frac{\partial(\rho\alpha_l)}{\partial t} + \nabla \cdot (\alpha_l \rho \mathbf{u}_l) \right) + \frac{1}{\rho} \left(\frac{\partial(\rho\alpha_v)}{\partial t} + \nabla \cdot (\alpha_v \rho \mathbf{u}_v) \right) = \Gamma_{lv} \left(\frac{1}{\rho_l} + \frac{1}{\rho_v} \right) \quad (1)$$

where subscripts *v* and *l* correspond respectively to the vapor and liquid phases and Γ_{lv} is the mass transfer by unit volume which is being vaporized. It is calculated at each time step through a simplified Rayleigh-Plesset equation ($\Gamma_{lv} = \dot{m}^+ + \dot{m}^-$) assuming a shared pressure field, adapted both for vaporization (\dot{m}^+) and condensation (\dot{m}^-):

$$\dot{m}^+ = C_{vap} \frac{3\alpha_{nuc}(1-\alpha_v)\rho_v}{R_{nuc}} \left(\frac{2}{3} \frac{p_v - p}{\rho_l} \right)^{\frac{1}{2}} \quad (p < p_v) \quad (2)$$

$$\dot{m}^- = C_{cond} \frac{3\alpha_v \rho_v}{R_b} \left(\frac{2}{3} \frac{p - p_v}{\rho_l} \right)^{\frac{1}{2}} \quad (p > p_v) \quad (3)$$

where, C_{vap} , C_{cond} , α_{nuc} , R_{nuc} , R_b are constants that are defined in the solver's documentation [11]. In the inhomogeneous approach, interphase momentum transfer is accounted for via additional terms in the Navier-Stokes equations, shown in Equations 4 and 5:

$$\frac{\partial(\rho\alpha_l \mathbf{u}_l)}{\partial t} + \nabla \cdot (\alpha_l (\rho_l \mathbf{u}_l; \mathbf{u}_l)) = -\alpha_l \nabla p + \nabla \cdot (\alpha_l \mu_{eff} (\nabla \mathbf{u}_l + (\nabla \mathbf{u}_l)^T)) + \mathbf{M}_l - \Gamma_{lv} (\mathbf{u}_l - \mathbf{u}_v) \quad (4)$$

*Corresponding author: Dumas G, LMFN Lab, Mechanical Engineering Department, Laval University, Quebec, QC G1V 0A6, Canada, Tel: +1 418-656-213; E-mail: gduumas@gmc.ulaval.ca

Received October 26, 2016; Accepted December 05, 2016; Published December 10, 2016

Citation: Cote P, Dumas G (2016) Assessment of the Homogeneous Approach to Predict Unsteady Flow Characteristics of Sheet and Cloud Cavitation. J Appl Mech Eng 5: 242. doi: 10.4172/2168-9873.1000242

Copyright: © 2016 Cote P, et al. This is an open-access article distributed under the terms of the Creative Commons Attribution License, which permits unrestricted use, distribution, and reproduction in any medium, provided the original author and source are credited.

$$\frac{\partial(\rho_v \alpha_v \mathbf{u}_v)}{\partial t} + \nabla \cdot (\alpha_v (\rho_v \mathbf{u}_v; \mathbf{u}_v)) = -\alpha_v \nabla p + \nabla \cdot (\alpha_v \mu_{eff} (\nabla \mathbf{u}_v + (\nabla \mathbf{u}_v)^T)) + \mathbf{M}_v - \Gamma_{lv} (\mathbf{u}_l - \mathbf{u}_v) \quad (5)$$

where μ_{eff} is the effective viscosity ($\mu_{eff} = \mu + \mu_t$), as expressed by the Boussinesq assumption and modeled in this work via a standard $k - \omega$ SST turbulence model. In Equations (4) and (5), \mathbf{M} is the force acting on a phase due to the presence of the other (i.e. drag; $\mathbf{M}_v = -\mathbf{M}_l$). By using a volume of fluid (VOF) approach to represent transport phenomena at the interface, one can use the interfacial area $A_{lv} = |\nabla \alpha_v|$ to calculate the drag force exerted at the interface:

$$\mathbf{M}_v = C_D \rho_m A_{lv} |\mathbf{u}_l - \mathbf{u}_v| (\mathbf{u}_l - \mathbf{u}_v) \quad (6)$$

where $C_D = 0.44$, which corresponds to the drag coefficient of spherical particles in Newton's regime, independent of the Reynolds number [11].

A homogeneous approach to simulate multiphase flows relies on the assumption of a mixture, simply characterized by a volume density $\rho_m = \alpha_v \rho_v + (1 - \alpha_v) \rho_l$ in which the velocity, turbulence fluctuations and temperature are shared homogeneously. With such assumptions, one can rearrange equations (4) and (5) to obtain the Navier-Stokes equation of the mixture:

$$\frac{\partial(\rho_m \mathbf{u})}{\partial t} + \nabla \cdot (\rho_m \mathbf{u}; \mathbf{u}) = \nabla p + \nabla \cdot (\mu_{eff} (\nabla \mathbf{u} + (\nabla \mathbf{u})^T)) \quad (7)$$

Experimental Cases and their Numerical Representation

Two different 2-D geometries are proposed for comparison with simulations (Figure 1). The first geometry corresponds to a cavitation tunnel studied by Leroux and Astolfi [13-15], in which a c chord NACA hydrofoil is positioned at a 6° angle of attack. The second case consists of an 8° throat venturi geometry studied by Barre and

Aeschlimann [16,17]. For both cases, space and time variables are hereafter normalized respectively with reference length and convective time-scale as x/L and $t^* = t/(L/U_\infty)$.

Boundary conditions and numerical representation

To correctly represent both experimental setups, boundary conditions are set with great care after relevant validations [18]. As shown at the left of Figure 1, 20 chord length extensions are set upstream and downstream of the hydrofoil. The walls of the tunnel are modeled as slip free walls, without considerations for viscous effects. A total pressure condition is set at the inlet along with an averaged absolute pressure outlet, controlling the value computed which is defined as:

$$\sigma = \frac{p_\infty - p_v}{\frac{1}{2} \rho U_\infty^2} \quad (8)$$

where the actual velocity, and thus Reynolds number, are results of the simulation. For the venturi geometry, a velocity inlet is used along with an averaged absolute pressure outlet. The inlet total pressure therefore becomes part of the solution.

In this work, regimes of both sheet and cloud cavitation are simulated on the foil geometry (cases "Sheet-foil" and "Cloud-foil"), while the venturi geometry is simulated only in an unstable manner (case "Cloud-venturi"). For a quick review of the regimes of cavitation, one can refer to the experimental works of Arndt or Leroux [13]. The specific details of the experimental and numerical setups are given below in Table 1. Both numerical setups along with their respective boundary conditions are shown in Figure 1.

For the foil geometry, the proposed numerical mesh is composed of nearly 146 000 elements and allows for a good resolution in the cavity area and in the wake region. For the venturi geometry, the retained

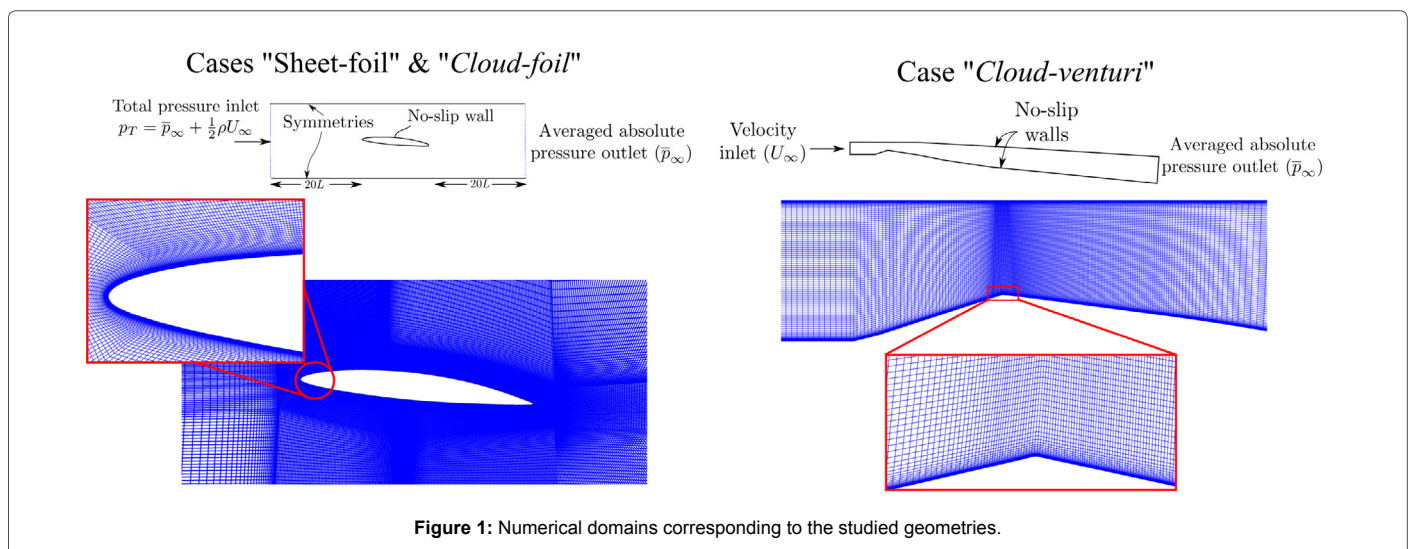


Figure 1: Numerical domains corresponding to the studied geometries.

Parameter	Sheet-foil	Cloud-foil	Cloud-venturi
Inlet velocity U_∞ (m/s)	4.76	4.76	7.04
Exp. cavitation number σ (-)	1.34	1.25	2.15
Exp. cloud shedding frequency (Hz)	n/a	3.5	45
Reference length (chord/venturi throat length) (m)	0.15	0.15	0.224
Reynolds number Re (-)	0.8×10^6	0.8×10^6	1.6×10^6

Table 1: Experimental conditions of the studied cases.

structured mesh contains a total of 50 000 elements and is also properly adapted in the vapor cavity area. To assess the unsteady behavior of the cavitating flow, pressure probes are positioned in both cases as in the experiments.

The unsteady simulations progress in time at a reduced discrete time step of $dt^* = 0.01$. Each unsteady simulation is initialized with the steady state, single phase flow solution in absolute pressure conditions. During the simulation, probes capture an absolute pressure signal that is transformed into a pressure coefficient. The time-averaged and RMS values are then calculated by eliminating the transient time of the cavity formation [18]. For all cases, the proper statistical convergence of unsteady flow characteristics was systematically verified.

The simulations performed under the venturi geometry use a “High resolution” advection scheme while calculations done on the foil geometry use a 2nd order upstream advection scheme. Depending on the ease of convergence, adjustments were done on the residuals convergence criteria. A thorough validation of the methodology proposed here has been carried out and is presented in [18].

Homogeneous Simulations of Sheet and Cloud Cavitation

When simulating sheet cavitation with a homogeneous approach, one rapidly notices that certain aspects of the physics associated to the re-entrant jet underneath the vapor cavity are discarded due to the underlying assumptions of a shared momentum field. In Figure 2 for example, the flow field surrounding the sheet cavitation vapor cavity is shown both with velocity streamlines (left) and with the reduced vorticity (right).

To facilitate interpretation of Figure 2, arrows have been added to point to the areas of interest. Near the leading edge of the foil at the left, the flow separates slightly because of the incidence which leads to the formation of a region of pure vapor inside the separation bubble ($\alpha_v \approx 1$). In the closure region of the cavity, the re-entrant jet is visible as the liquid flowing near the wall moves toward the leading edge of the cavity. At that particular location, an important velocity gradient is created between the low velocity re-entrant jet, near the wall, and the free stream velocity over the cavity.

One can see at the right of Figure 2 that in the homogeneous approach, the boundary layer develops on the hydrofoil wall as it would in a non-cavitating simulation. In the closure region of the cavity,

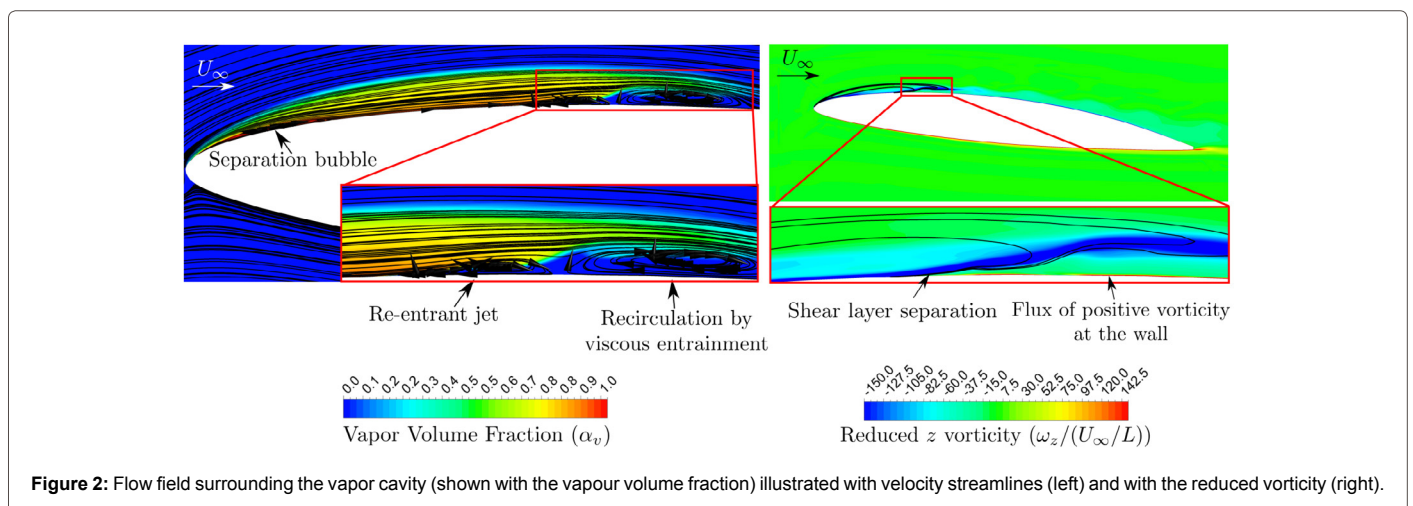
where an adverse pressure gradient allows the pressure to reach non-cavitating conditions, the shear layer detaches from the foil. Finally, one can note that the region under the separated shear layer contains positive vorticity ($\omega_z > 0$), related to the presence of the re-entrant jet.

One could argue that the physics simulated here is not representative of what would be observed in experiments. The presence of vapor at the leading edge would indeed modify the effective body of the foil. The boundary layer, forming at the leading edge, would then develop on top of the liquid-vapor interface and contribute to the formation of the re-entrant jet by the diffusion of vorticity in the cavity closure region. This would indeed be closer to the experimental observations of Franc and Michel [19,20], Callenaere [21] and Kawanami [22]. However, even if the local flow field surrounding the cavity is not precisely simulated with respect to the existence of a modified effective body, the time-averaged pressure distribution and the RMS distribution of the pressure fluctuations for both sheet and cloud cavitation on the foil are found to match fairly well with experiments, as shown in Figure 3.

It can be observed in Figure 3 that the time-averaged pressure distributions match quite well with the experimental data obtained by Leroux for both cases. As is the case with experiments for sheet cavitation ($\sigma = 1.34$), inside the cavity the pressure is mostly constant and equal to the vapor pressure ($C_p \approx -\sigma$).

When going further toward the trailing edge, an adverse pressure gradient allows the pressure to reach non-cavitating conditions. Again, as was observed experimentally, this recompression is associated with an increase in the pressure fluctuations amplitude, which is greatest in the cavity closure region. Regarding the “Cloud-foil” case, one can notice that even though the shape of the pressure distribution matches fairly well with experiments, it is slightly closer to the non-cavitating pressure distribution than to experiments.

At the bottom of Figure 3, one can see for the “Sheet-foil” case that the amplitude of the fluctuations is over predicted from the cavity closure ($x/L = 0.5$) to the trailing edge of the foil. As mentioned by Leroux, inside the cavity, the pressure fluctuations are mostly constant and equal the fluctuations measured in non-cavitating conditions. These are well predicted by the simulations. However, for the case of cloud cavitation, the pressure fluctuations are greatly over predicted in the vicinity of the leading edge ($x/L < 0.4$). From mid-chord to the trailing edge, the fluctuations distribution is again over predicted but the shape of the latter better matches the experimental data.



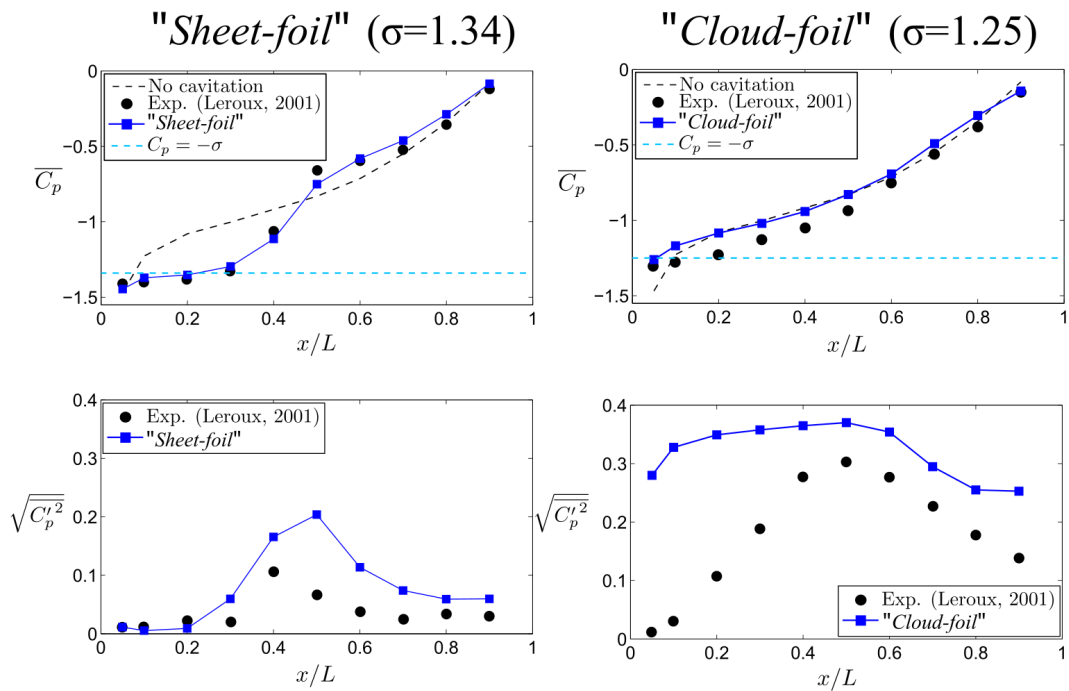


Figure 3: Time-averaged pressure distribution and RMS distribution of the pressure fluctuations on the suction side of the hydrofoil for both sheet (left) and cloud (right) cavitation case.

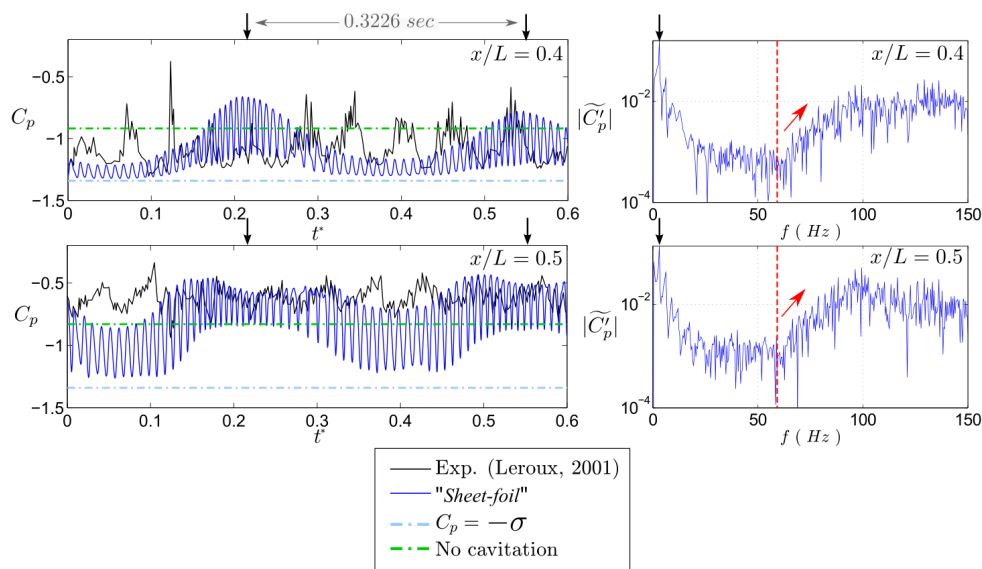


Figure 4: At the left, time evolution of the pressure signals at $x/L = 0.4$ and $x/L = 0.5$ for the case of sheet cavitation on the foil. At the right, corresponding frequency domain is analysed. Black arrows show the low frequency fluctuations peaks on the time evolution signal and their corresponding frequency at the right. The red lines and red arrows show the increase in energy caused by the higher frequency fluctuations.

For both cases, experimental pressure signals were measured on the foil, which helps to gain a better understanding of the computed and experimental physics. For the simulated cases, FFT analyses allow the frequency domain content of the time domain signals to be obtained. The resulting signals and frequency contents for the case of sheet cavitation on the foil, at resulting signals and frequency contents

for the case of sheet cavitation on $x/L = 0.4$ and $x/L = 0.5$ in the cavity closure region, are presented in Figure 4.

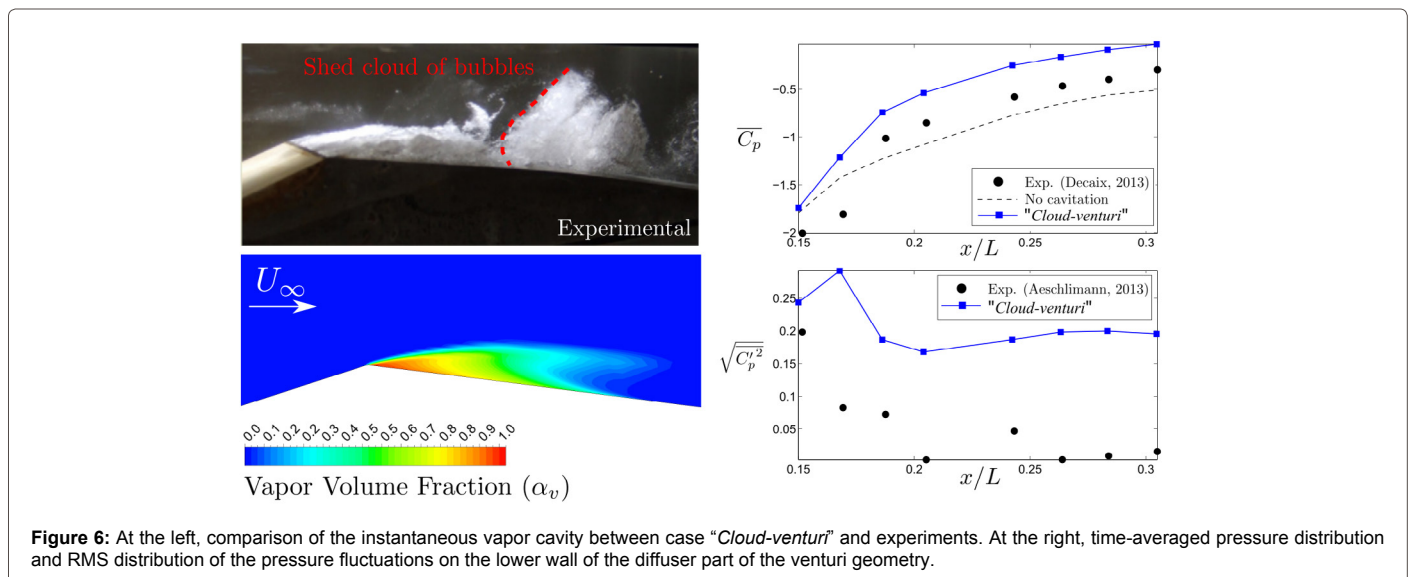
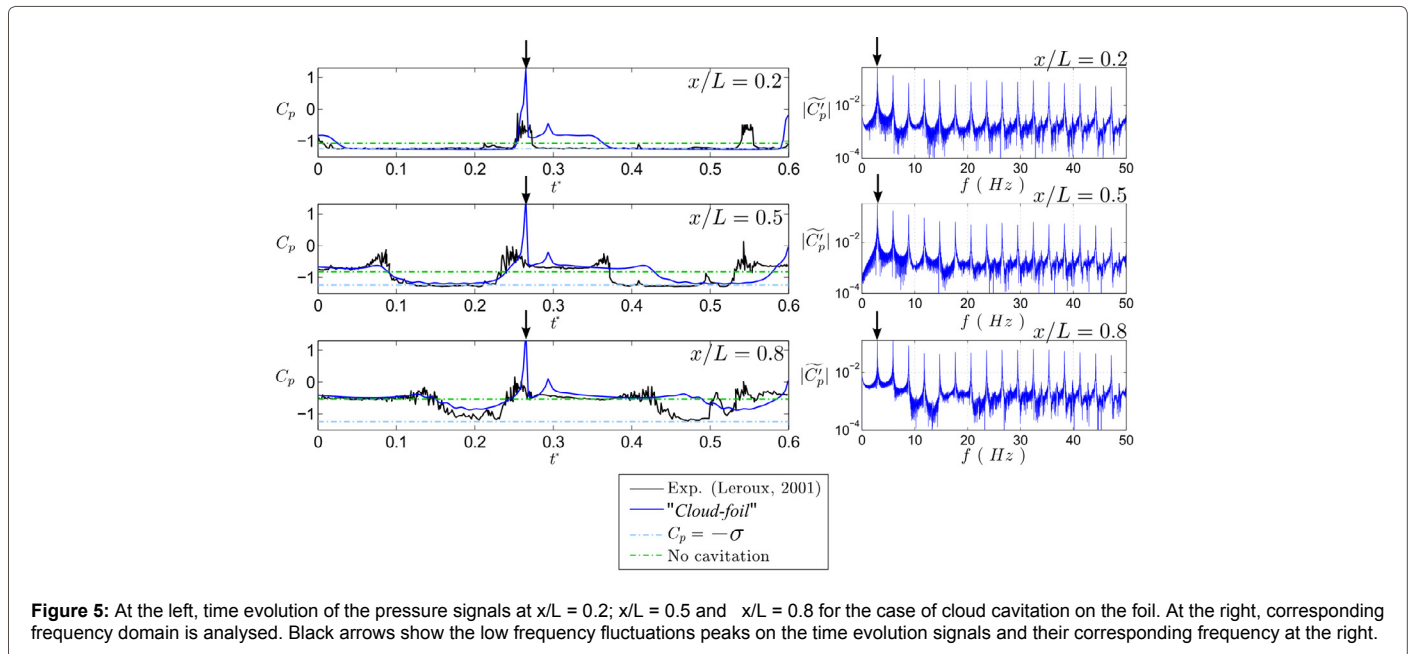
It appears from Figure 4 that the unsteady flow that is simulated is not in agreement with what is being observed experimentally. The pressure signal obtained in the simulation contains high amplitude,

low frequency content that is shown in the left of Figure 4 with black arrows. In the right of Figure 4, the black arrow shows the frequency corresponding to this movement at $f = 3.10$ Hz. We can also observe that the experimental data does not possess this low frequency behavior. In experiments, the signal contains energy at medium frequencies ($f = 18.75$ Hz) plus weaker fluctuations at higher frequencies. As shown in the right of Figure 4, the numerical signal also contains energy at higher frequencies with great amplitudes. This tends to create a camber in the frequency spectrum from around $f = 60$ Hz and above, as shown with the red lines and arrows.

One can also note on the upper left plot of Figure 4 that the pressure coefficient at $x/L = 0.4$ varies between the value without cavitation (shown with the dashed green line) to a value slightly above the vapor pressure ($C_p = -\sigma$, in the dashed blue line). This suggests a movement of the cavity closure caused by the instability of attached cavitation. It also suggests that the simulated cavity possesses two

different pulsating behaviors. First, the cavity shows a large movement of its closure position, generating the fluctuations of lower frequencies. Secondly, it appears that the pressure fluctuations of higher frequencies are not caused by the movement of the cavity closure region itself but rather by the whole flow around the foil. Unsteady visualizations of the numerical simulation help to validate this last point. The same time-frequency signal analysis is proposed below in Figure 5 for the case of cloud cavitation on the foil.

As one can see in the middle of Figure 5 ($x/L = 0.5$), the self-oscillating behavior of the vapor cavity is easily visible as the pressure oscillates from the saturated pressure value ($C_p = -\sigma$, blue dashed line) to the value without cavitation (dashed green line). The phenomenon repeats itself at a frequency of $f = 2.96$ Hz (shown with the black arrow at the right of Figure 5) and is associated with the collapse of the cavity which generates a strong pressure pulsation (pointed with a black arrow, left of Figure 5). In the experiments, this behavior is characterized by



a frequency of $f = 3.5$ and leads to a strong fluid-structure interaction phenomenon. The latter can be explained by the important quantity of energy that is contained in the pressure fluctuations and their harmonics, as shown at the right of Figure 5.

Regarding the computations done on the venturi geometry, the flow field surrounding the instantaneous vapor cavity of case “Cloud-venturi” is shown in Figure 6.

One can see at the left of Figure 6 that the location, shape, and amount of vapor appears to be in relative agreement with the experimental observation, if one excludes the cloud of bubbles that was just shed by the main cavity. However, one can also see at the right of Figure 6 that calculations are not as successful in predicting the time-averaged and unsteady characteristics of the cloud cavitation regime in the venturi geometry as it is in the case of the foil geometry.

The unsteady shedding behavior of cloud cavitation was reproduced in the simulations at a frequency of 19.2 Hz, well below the measurements (45 Hz). The phenomenon rapidly appeared very energetic, which caused numerical instability problems. As was the case with “Cloud-foil”, but now with a greater importance, the pressure pulsation that periodically appears (as pointed with a black arrow, left of Figure 5), leads to the over prediction of both the time-averaged and the RMS of the pressure shown in Figure 6 (as it was the case for “Cloud-foil”, bottom right of Figure 3). A certain amount of effort in assessing the best practices from the literature to produce more accurate results was done, as proposed by Zwart [9] and Coutier-Delgosha [5,6,15], but without any success [18].

For all cases studied in this work, despite being able to predict the shape and location of vapor and the physical mechanisms in cause, the methodology proposed does not allow the accurate prediction of the unsteady flow characteristics caused by attached cavitation. The model’s inability might cause this to reproduce the underlying physics of the re-entrant jet, as it was discussed in relation to Figure 2. The next sections now present simulations performed with the inhomogeneous approach on a case of sheet cavitation to identify what physics the consideration of an interface may induce.

Comparisons with the Inhomogeneous Approach

By using the inhomogeneous model included in ANSYS CFX (described in equations 4 and 5), a higher σ case ($\sigma = 1.72$) of sheet cavitation is simulated on the foil geometry. Numerical stability rapidly became problematic with the inhomogeneous approach. It was indeed not possible to simulate lower σ cases because of numerical divergence. For the two new cases of the flow around the foil, the time step is set to $dt^* = 0.05$ and a lighter mesh of 50 000 elements is used, both to improve numerical convergence. For both cases, the statistical convergence of unsteady flow characteristics was validated. The comparison of both homogeneous (“HOM”) and inhomogeneous (“INH”) cases of the foil at $\sigma = 1.72$ are presented below in Figure 7 with the reduced vorticity and vapor volume fraction contours. It appears that with the homogeneous approach, only a small region of the leading edge is filled with pure vapor. This is in contrast with the inhomogeneous approach in which a larger amount of vapor is found at the leading edge of the foil, which also better fits the qualitative experimental observations

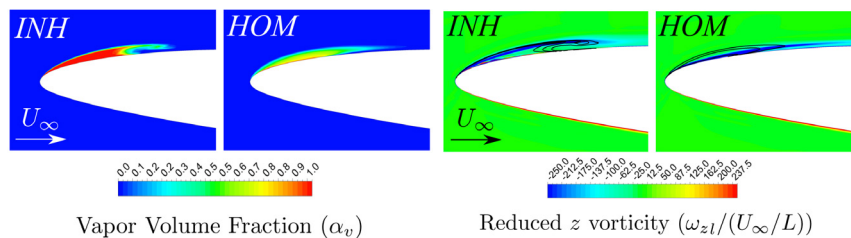


Figure 7: Flow field computed with both the inhomogeneous (“INH”) and homogeneous (“HOM”) approaches on the foil geometry at $\sigma = 1.72$. At the left is the instantaneous vapour volume fraction and at the right, the reduced vorticity.

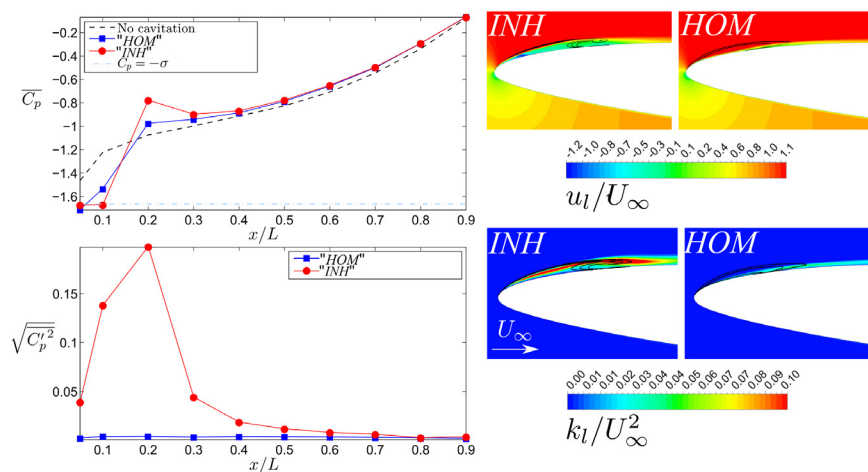


Figure 8: At the left, time-averaged pressure and RMS of the pressure fluctuations distributions for both homogeneous (“HOM”) and inhomogeneous (“INH”) cases. At the right, flow field surrounding the vapor cavity, shown by the liquid velocity and turbulent kinetic energy.

of Leroux [13]. For reminder, one of the highlighted problematics of the homogeneous approach, as identified in this work, is the lack of modification to the effective body by the presence of vapor. As observed at the right of Figure 7, the vorticity contours clearly show that with the inhomogeneous approach, the presence of vapor modifies the effective body encountered by the liquid flow, as the boundary layer develops at the water-vapor interface. As shown below in Figure 8, even though the resulting time-averaged pressure distributions are quite similar, the resulting different flow topology around the cavity leads to a significantly different RMS distribution of the pressure fluctuations.

One can see in the left of Figure 8 that both cases “*HOM*” and “*INH*” give slightly different time-averaged pressure distributions inside the vapor cavity. Resulting from this, the adverse pressure gradient, which allows the flow to return to non-cavitating conditions, is stronger when using the inhomogeneous approach. One can finally observe that the flow simulated with the homogeneous approach is very calm and generates almost no pressure fluctuations while considerable fluctuations are induced in the closure region with the inhomogeneous approach, possibly caused by the greater adverse pressure gradient.

It can be seen at the top right of Figure 8 that inside and downstream of the vapor cavity, the liquid velocity is greatly reduced as the effective body of the foil is modified. As shown in the bottom right of Figure 8, the resultant effective body leads to the detachment of the boundary layer, which rolls up and diffuses over the vapor cavity, as was experimentally observed by Gopalan and Katz [23]. On the other side, it appears that the small and late separation of the shear layer, downstream of the cavity in case “*HOM*”, only leads to a slight increase in the turbulent energy level.

While no experimental data are available for validation at $\sigma = 1.72$, the present investigation is quite revealing when considering the simulated physics. It was demonstrated that the modification of the body is only effective when using the inhomogeneous approach as per Figure 7, on the vorticity plot, showing the shear layer developing on the interface rather than at the wall. In the homogeneous approach, the two-phase mixture is indeed considered as a continuous medium. Although no detailed time evolutions of the pressure signal were available, the vorticity injected by the detached shear layer is expected to induce a richer dynamic behavior in the closure region of the cavity, which is suspected to play a considerable role in the spectral response of unsteady cavitation.

This also suggests that locally in the cavity area, the hypothesis of a continuous medium may not be appropriate. In fact, close to the foil, the presence of vapor tends to modify the effective body encountered by the liquid flow. The unsteady physics resulting from this phenomenon may therefore only be characterized with an inhomogeneous approach as they are partly associated with the vortical motion caused by the resulting modified body. Thus, it appears that the consideration of an interface might be critical in assessing the fine characteristics of unsteady cavitating flows.

Conclusion

Through this work, the capacity of the homogeneous approach to solve cavitating flows and predict the resulting unsteady flow characteristics, when used with the Rayleigh-Plesset cavitation model, has been assessed. By performing simulations on two relevant geometries, it was shown that the location, the shape and amount of vapor was always qualitatively close to experimental observations. For the foil geometry, the proposed methodology resulted in accurate time-averaged results for both sheet and cloud cavitation regimes.

However, for the venturi geometry, both time-averaged and unsteady pressure characteristics were amplified by the numerical pressure pulsations associated with the collapse. It was further observed that the homogeneous approach greatly simplifies the flow field surrounding the cavity, whereas the body encountered by the flow is not modified by the appearance of vapor at the leading edge. It is suggested that the vortical motions associated with the modified body would contribute to the proper unsteady response of cavitation.

By using a more complex numerical implementation, solving the flow as an inhomogeneous medium, it was found that with such a model, both phases share an interface. Therefore, the effective body of the foil becomes altered by the presence of vapor, which leads to a more complex but more physically relevant flow field around the vapor cavity. Numerical instability issues however limited the possibility to compare with experimental data and thus to further study the computed physics. More algorithmic developments in the simulation of inhomogeneous cavitation (with the free surface or VOF approach) should aim at rendering the method more numerically robust. This would allow comparisons of simulations of attached cavitation with detailed experimental data, and thus, the capabilities of the inhomogeneous approach could be clearly evaluated. However, from the physics at play, it clearly appears that inhomogeneous simulations of cavitation could lead to better predictions of unsteady characteristics of cavitation. However, for applications into hydraulic machinery, it appears not possible now to accurately predict unsteady flow characteristics caused by cavitation in a robust and general manner.

Acknowledgments

The authors would like to thank the FRQNT and NSERC for their financial support of this research project. Computations were performed on the Colosse supercomputer at Laval University, under the auspices of Calcul Québec and Compute Canada.

References

1. Dörfler P, Sick M, Coutu A (2013) Flow-induced pulsation and vibration in hydroelectric machinery. Springer.
2. Yamamoto K, Müller A, Favrel A, Landry C, Avellan F (2014) Pressure measurements and high speed visualizations of the cavitation phenomena at deep part load condition in a Francis turbine. In 27th IAHR Symposium on Hydraulic Machinery and Systems, Number 22 in IOP Conference Series: Earth and Environmental Science.
3. Lowys PY, Paquet F, Couston M, Farhat M, Natal S, et al. (2002) Onboard measurements of pressure and strain fluctuations in a model of low head francis turbine - part 2: measurements and preliminary analysis results. In Proceedings of the Hydraulic Machinery and Systems 21st IAHR Symposium: 873-880.
4. Arndt REA, Song CCS, Kjeldsen M, Keller A (2000) Instability of partial cavitation: A numerical/experimental approach. In The Proceedings of the Twenty-Third Symposium on Naval Hydrodynamics.
5. Coutier-Delgosha O, Stutz B, Vabre A, Legoupil S (2007) Analysis of cavitating flow structure by experimental and numerical investigations. J Fluid Mechanics 578: 171-222.
6. Coutier-Delgosha O, Fortes-Patella R, Reboud JL (2003) Evaluation of the turbulence model influence on the numerical simulations of unsteady cavitation. J. Fluids Eng 125: 38-45.
7. Frikha S, Coutier-Delgosha O, Astolfi JA (2008) Influence of the cavitation model on the simulation of cloud cavitation on 2d foil section. Int J Rotating Machinery 2008: 12.
8. Huang DB, Young YL (2012) Numerical modeling of unsteady cavitating flows around a stationary hydrofoil. Int J of rotating machinery 2012: 17.
9. Zwart P, Gerber AG, Belamri T (2004) A two-phase flow model for predicting cavitation dynamics. In ICMF 2004 International Conference on Multiphase Flow.
10. Brennen C (2005) Fundamentals of multiphase flows. Cambridge University Press.

11. ANSYS (2012) ANSYS CFX-Solver Modelling Guide. ANSYS.
12. ANSYS (2012) ANSYS CFX-Solver theory guide. ANSYS Inc release.
13. Leroux JB, Astolfi JA, Billard JY (2001) An experimental investigation of partial cavitation on a two-dimensional hydrofoil. In the Proceedings of the Fourth International Symposium on Cavitation.
14. Leroux JB, Coutier-Delgosha O, Astolfi JA (2005) A joint experimental and numerical study of mechanisms associated to instability of partial cavitation on two-dimensional hydrofoil. *Physics of fluids* 17: 052101.
15. Coutier-Delgosha O, Fortes-Patella R, Reboud JL, Stutz B (2002) Test case number 30: Unsteady cavitation in a venturi type section (pn).
16. Barre S, Rolland J, Boitel G, Goncalves E, Fortes Patella R (2009) Experiments and modeling of cavitating flows in venturi: Attached sheet cavitation. *European J Mechanics B/Fluids* 28: 444-464.
17. Aeschlimann V, Barre S, Djeridi H (2013) Unsteady cavitation analysis using phase averaging and conditional approaches in a 2D venturi flow. *Open J Fluid Dynamics* 3: 171-183.
18. Côté P (2015) Investigation of the self-excited vibrations in a Francis runner in transient conditions of load rejection. Master's thesis, Département de génie mécanique, Université Laval.
19. Franc JP, Michel JM (1985) Attached cavitation and the boundary layer: Experimental investigation and numerical treatment. *J Fluid Mechanics* 154: 63-90.
20. Franc JP (2001) Partial cavity instabilities and re-entrant jet. In The Proceedings of the Fourth International Symposium on Cavitation
21. Callenaere M, Franc JP, Michel JM (1998) Influence of cavity thickness and pressure gradients on the unsteady behavior of partial cavities. In The Proceedings of the Third International Symposium on Cavitation.
22. Kawanami Y, Kato H, Yamaguchi H, Tanimura M, Tagaya Y (1997) Mechanism and control of cloud cavitation. *J Fluids Eng* 119: 788-794.
23. Gopalan S, Katz J (2000) Flow structure and modeling issues in the closure region of attached cavitation 12: 895.